Dynamic Current Distribution in the Electrodes of Submerged Arc Furnace Using Scalar and Vector Potentials

Yonatan Afework Tesfahunegn[1(✉)], Thordur Magnusson[2], Merete Tangstad[3], and Gudrun Saevarsdottir[4]

[1] Engineering Optimization and Modeling Center, School of Science and Engineering, Reykjavik University, Mentavegur 1, 101 Reykjavik, Iceland
yonatant@ru.is
[2] United Silicon, Stakksbraut 9, 230 Reykjanesbæ, Iceland
tm@silicon.is
[3] Department of Materials Science and Engineering, NTNU, 7491 Trondheim, Norway
merete.tangstad@ntnu.no
[4] School of Science and Engineering, Reykjavik University, Menntavegur 1, 101 Reykjavik, Iceland
gudrunsa@ru.is

Abstract. This work presents computations of electric current distributions inside an industrial submerged arc furnace. A 3D model has been developed in ANSYS Fluent that solves Maxwell's equations based on scalar and vector potentials approach that are treated as transport equations. In this paper, the approach is described in detail and numerical simulations are performed on an industrial three-phase submerged arc furnace. The current distributions within electrodes due to skin and proximity effects are presented. The results show that the proposed method adequately models these phenomena.

Keywords: Current distribution · Skin effect · Proximity effect
Submerged arc furnace

1 Introduction

Current distribution is critical for proper operation of Submerged Arc Furnaces for silicon production. Control systems do not offer this information as it is not directly measurable, but metallurgists operate furnaces based on experienced interpretation of available data. A number of recent dig-outs of industrial furnaces have expanded available information on location-dependent charge properties, thus enabling numerical models with reasonably realistic domain configurations. This has the potential to enhance understanding of critical process parameters allowing more accurate furnace control.

A masters thesis by Krokstad [1] published in 2014 describes measurements of the electrical conductivity of silicon carbide and Vangskåsen [2] in 2012 looked in detail at

Y. Shi et al. (Eds.): ICCS 2018, LNCS 10861, pp. 518–527, 2018.
https://doi.org/10.1007/978-3-319-93701-4_40

the metal producing mechanisms. Molnas [3] and Nell [4] have also published data on digout samples and material analysis that are relevant. These are some of the basic components necessary to set up a reasonably realistic modeling domain with correct physical properties to model the current distribution within a furnace, and therefore there is now a unique opportunity to create a model which enables understanding of the current distribution in the furnace. These results can be used in the development of furnace control strategies that can allow improved silicon recovery and current efficiency.

A number of researchers have published results on current distribution of Submerged Arc Furnaces using Finite Volume Method (FVM) and Finite Element Method (FEM). Palsson and Jonsson [5] used FEM to analyze the skin and proximity effects in Soderberg electrodes for FeSi furnace. In the paper, a cross-section of the furnace is modeled in 2D and solved to obtain a time-harmonic solution of AC currents in the electrodes. Toh *et al.* [6] used FVM to model steelmaking process. In their approach, they follow scalar and vector potentials to implement Maxwell's equations. Diahnaut [7] presented computations of the electric field in SAF using CFD. The author showed the effect of contact resistance by studying the contact between two coke particles before dealing with a full-scale furnace. The furnace was partitioned into layers to consider different materials, and no assumptions were made regarding the current path. Bezuidenhout *et al.* [8] applied CFD on a three-phase electric smelting furnace to investigate the electrical aspects, thermal and flow behavior. They showed relationships between electrode positions, current distribution and slag electrical resistivity. Darmana *et al.* [9] developed a modeling concept applicable for SAFs using CFD that considers various physical phenomena such as thermodynamics, electricity, hydrodynamics, heat radiation and chemical reactions. Wang *et al.* [10] investigated the thermal behavior inside three different electric furnaces for MgO production.

This paper presents computations of electric current distributions inside an industrial submerged arc furnace. A 3D model has been developed in ANSYS Fluent [11] that solves Maxwell's equations based on scalar and vector potentials approach that are treated as transport equations. They are implemented using User Define Scalar (UDS). In the next sections, the process of producing silicon, and the proposed approach are described in detail. The proposed methodology is applied to an industrial three-phase submerged arc furnace. At this stage, not all the furnace components are included in the analysis. Only the three electrodes and the outer boundary of the furnace are considered. Hence, the current distributions within the electrodes due to skin-effect (current flowing near the electrode surface) and proximity-effect are presented.

2 The Process

In the silicon production process, quartz and carbon materials are fed into a Submerged Arc Furnace. The raw material mix fills up the furnace and forms a charge. Three electrodes sticking into the charge from above. The energy for the reactions in the furnace is provided by electric heating from the current passed to the furnace through the electrodes, but each carries one of three phases of 50 Hz AC current, canceling out at a star-point in the furnace.

The overall reaction for producing Silicon metal is:

$$SiO_2 + 2C = Si + 2CO(g) \quad (1)$$

This reaction, however, happens through a series of sub-reactions, changing the properties of the charge along the way as intermediary reaction products are formed. The current passes from the electrodes through the raw-material charge and an electric arc burning at the tip of the electrode. The arc, which consists of thermal plasma in the range of 10000–30000 K provides heat for energy consuming silicon producing reaction (4) while the SiC forming reaction and SiO(g) condensation, reactions (2) and (3), happen at a lower temperature further up in the furnace [12]:

$$SiO(g) + 2C = SiC + CO(g) \quad (2)$$

$$2SiO(g) = Si + SiO_2 \quad (3)$$

$$SiO_2 + SiC = SiO(g) + CO(g) + Si(1) \quad (4)$$

It is extremely important for the silicon recovery in this process that there is a balance between the high temperature reactions (4) and the low temperature reactions (2) and (3). Therefore, it is necessary that sufficient heat is released in the arc, while a certain part should be released in the raw-material charge.

The current distribution is not well known for silicon furnaces, and cannot be directly measured. Saevarsdottir *et al.* [13] calculated that the arc could be maximum 10–15 cm, based on the electrical parameters. Although there have been publications on this subject, (for example [14]), no results from an accurate model where the current distribution can be calculated have been published to date.

The geometry of the zones in a silicon furnace depends on the operation history, and hence a number of different geometries, sizes and compositions are possible in various parts of the furnace. A report from recent excavations of industrial furnaces published by Tranell *et al*. [15] describe various zones in a FeSi furnace. Myrhaug [16] reported similar features from a pilot scale excavation operating around 150 kW. Tangstad *et al*. [17] published results from excavation of industrial furnaces, where the interior of the furnace is divided into zones depending on the materials and their degree of conversion. Mapping the material distribution gives a basis for quantifying the location-dependent physical properties of the charge materials such as the electrical conductivity.

3 Computational Model

In this section, we describe the mathematical modeling, the furnace geometry, material properties, mesh generation and boundary conditions.

3.1 Mathematical Modeling

In this paper, we will focus only on the electrical aspects of SAF. The 3D electrical model is developed in ANSYS Fluent [11] based on scalar and vector potentials approach to solve the Maxwell's equations. This will capture the time-dependent effects, the induction of magnetic field and the resulting magnetic forces in the system, but for the considerations in this paper, we will not deal with the magnetic forces. In the Maxwell's equations we have taken the following assumptions:

a. The current displacement is zero $\left(\frac{\partial \boldsymbol{D}}{\partial t} = 0\right)$. This is valid as the frequency of the AC-period is low (50 Hz).
b. Charge density is ignored which is the result of (a).

Hence the modified Maxwell's equations are the following [18]

$$\nabla \cdot \boldsymbol{B} = 0 \tag{5}$$

$$\nabla \times \boldsymbol{E} = -\frac{\partial \boldsymbol{B}}{\partial t} \tag{6}$$

$$\nabla \times \boldsymbol{B} = \mu \boldsymbol{J} \tag{7}$$

$$\nabla \cdot \boldsymbol{J} = 0 \tag{8}$$

From Ohm's law [18]:

$$\boldsymbol{J} = \sigma \boldsymbol{E} \tag{9}$$

where ***B, E, D***, ***J,*** μ and σ represent magnetic flux density, electric field, electric flux density, electric current density, magnetic permeability and electrical conductivity, respectively.

Introducing scalar and vector potentials, ϕ and $\boldsymbol{A}$ the unknowns in Maxwell's equations will be reduced from six (three components of $\boldsymbol{E}$ and $\boldsymbol{B}$) to four (ϕ and three components of $\boldsymbol{A}$). In the study of electromagnetism [18], especially when potentials are introduced two identities are important, i.e., the curl of the gradient of any scalar field is zero ($\nabla \times \nabla\phi = 0$), and the divergence of the curl of any vector field is zero ($\nabla \cdot \nabla \times \boldsymbol{A} = 0$). Hence after some manipulations and substitution, we get the following relationships:

$$\boldsymbol{E} = -\nabla\phi - \frac{\partial \boldsymbol{A}}{\partial t} \tag{10}$$

$$\boldsymbol{B} = \nabla \times \boldsymbol{A} \tag{11}$$

$$\nabla(\nabla \cdot \boldsymbol{A}) - \nabla^2 \boldsymbol{A} = \mu \boldsymbol{J} \tag{12}$$

Taking the divergence of Eq. (10) and assuming Coulomb condition ($\nabla \cdot \boldsymbol{A} = 0$) [18], we get the following equations:

$$\nabla^2 \phi = 0 \tag{13}$$

$$\sigma \frac{\partial \boldsymbol{A}}{\partial t} - \nabla \cdot \left(\frac{1}{\mu} \nabla \boldsymbol{A} \right) = -\sigma \nabla \phi \tag{14}$$

In Eq. (14) the gradient of the scalar potential is a source. Even though Eq. (13) is already implemented in ANSYS Fluent MHD module, it is not supported to impose time-varying voltage or current. Hence we need to develop four UDS transport equations to solve Eqs. (13) and (14). By using the distribution of scalar potential ϕ and of vector potential $\boldsymbol{A}$ obtained by solving Eqs. (13) and (14) with suitable boundary conditions, the following relation can calculate the distribution of electric current density.

$$\boldsymbol{J} = -\sigma \nabla \phi - \sigma \frac{\partial \boldsymbol{A}}{\partial t} \tag{15}$$

The distribution of magnetic flux density can be obtained by Eq. (11).

3.2 Furnace Geometry and Material Properties

To verify the proposed approach, it is suitable to use benchmark problems. However, there are no available benchmark problems that have either analytical or experimental solutions related to submerged arc furnaces. Palsson and Jonsson [5] have used a two-dimensional FEM model that has three electrodes. In their model, the variation along the axis of the electrodes is neglected. Hence, they considered a cross-sectional area of a furnace. In the FEM model, it is convenient to apply current at a node of the electrodes. In the FVM model it is not possible to impose current on a node. It should be applied normal to a surface area. This means that in this paper, a 3D FVM model should be created. To replicate the 2D model, the length of electrodes should be sufficiently long to make the effect of the boundary will be negligible. All simulation results of the simulation will be reported in the middle cross-section. The 3D domain is shown in Fig. 1. The dimensions of the the modeling domain are taken from [5].

The electrode electrical conductivity is assumed to be $\sigma = 3 \times 10^4$ and the relative permeability is $\mu_r = 1$. The conductivity and relative permeability in the furnace is 0 and 1 respectively.

3.3 Mesh Generation and Boundary Conditions

Mesh generation is a crucial part of any computational method. It has a significant influence on the runtime and memory use of simulation, as well as the accuracy and stability of the solution. The material volumes (electrodes and the furnace part) were meshed using ICEM-CFD [19]. The mesh is generated using unstructured grid. After performing preliminary grid convergence study, the minimum and maximum element sizes are set 5 and 30 cm, respectively. To reduce the cell count, the unstructured mesh is converted to a polyhedral mesh in ANSYS Fluent reducing the cell count by almost two thirds, thus enabling faster convergence and saving computational expense.

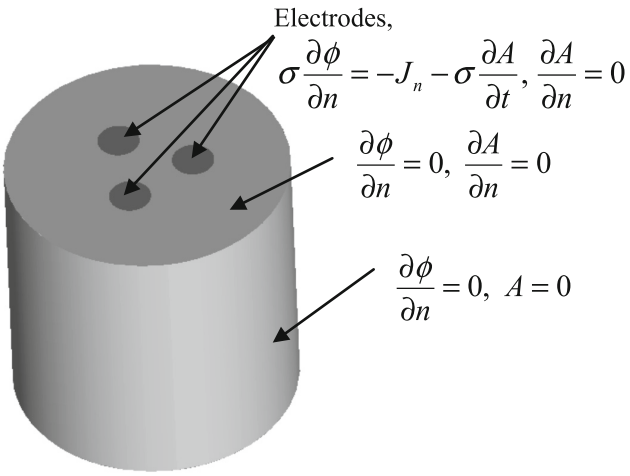

Fig. 1. Computational domain with boundary conditions

The boundary conditions are indicated as shown in Fig. 1. Note that the same boundary conditions are applied on the top and bottom surfaces of the furnace. It is assumed that there is no magnetic flux through the furnace wall. Applying such condition imposes that the vector potential **A** is constant, which involves the simple case **A** = 0 at the outer boundary. The boundary condition $\partial\phi/\partial n = 0$, where n is the normal vector on the outer side of the furnace combined with **A** = 0 imposes that there is no current flow out of the furnace.

The top and bottom surfaces of the electrodes defined as conductive walls by applying the respective phase currents as current density. Here, a total current density of 118 kA RMS [5] divided by the electrode cross-section area is applied on the top and the bottom surfaces of the electrodes but with a phase shift of 120° between them. Thus the current density on electrode k; k = 0, 1, 2 is

$$J_k = \frac{118}{A_e\sqrt{2}}\sin\left(2\pi ft + \frac{2\pi k}{3}\right) \tag{16}$$

where A_e, f and t are the cross-sectional area of electrode, frequency and time.

4 Results

In this section, we study the skin and proximity effects on the electrodes using the proposed method as described in Sect. 3. In this work, the frequency is taken as 50 Hz which is the standard frequency in furnace operation. The solver setup is a second order upwind scheme based on an implicit formulation. The iterative convergence of each solution is examined by monitoring the overall residual, which is the sum (over all the cells in the computational domain) of the L^2 norm (also known as least squares) of all the governing equations solved in each cell. The solution convergence criterion

throughout the simulation period is the one that occurs first of the following: a reduction of the residuals by eight orders of magnitude, or maximum iterations of 1000.

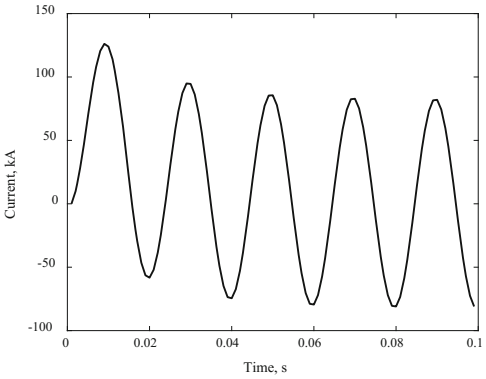

Fig. 2. Comparison between input and simulated current

To achieve reasonable and stable result, several simulations have been performed for over four periods. As it can be seen in Fig. 2, for the first three periods the current was unstable.

A grid convergence study has been conducted to discern the effect of grid refinement based on a total current. For the study, three different levels of grid refinements with time-step (Δt) of 0.001 have been considered. The three grids are coarse, medium and fine grids with total cells of 154829, 293476 and 486656, respectively. The results are shown in Fig. 3. The maximum difference between fine and coarse models is about 4.5 kA and between fine and medium is approximately 0.6 kA. Consequently, utilization of the medium grid will be sufficient for further analysis.

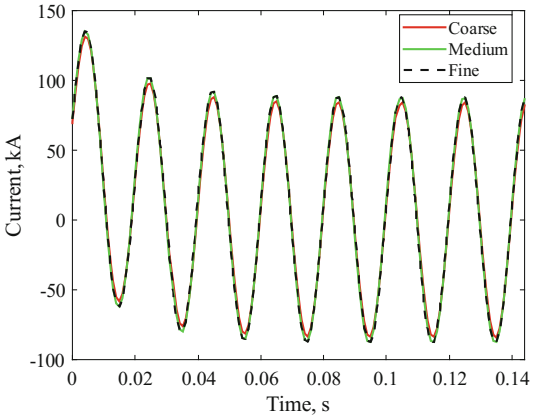

Fig. 3. Grid convergence study

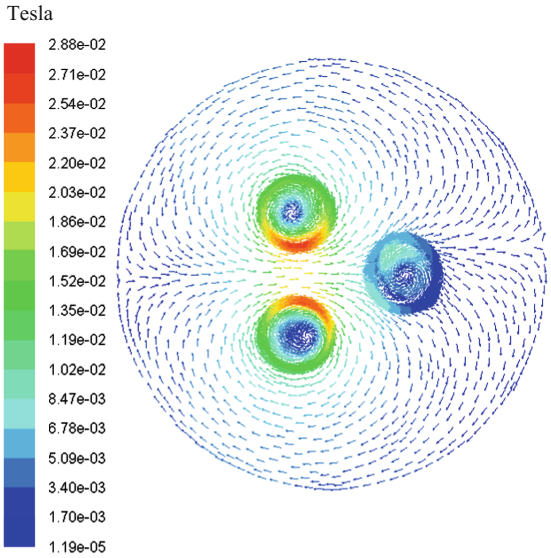

Fig. 4. Magnetic flux density in the middle section

Figure 4 shows the magnetic field in the cross-section of the furnace at one-time point. At this particular time, the two electrodes in the left have higher current but in opposite directions and less current is flowing through the third electrode. Figure 5 indicates the resulting non-uniform current distributions on the electrodes. The non-uniformity is the result of skin-effect and proximity-effect.

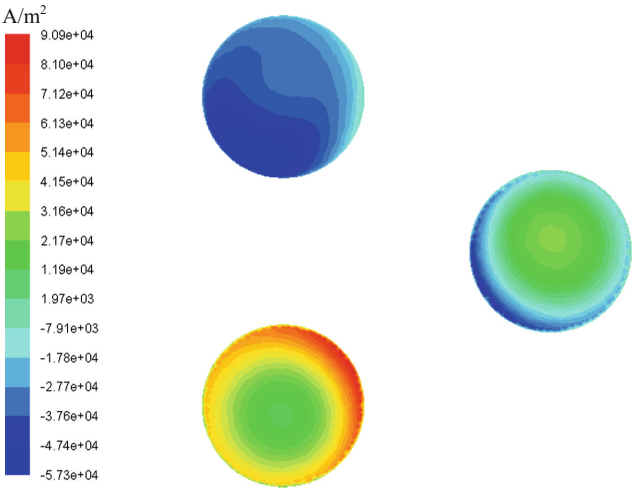

Fig. 5. Current densities within the three electrodes

5 Conclusions

This work proposed scalar and vector potentials approach to solve the time-dependent Maxwell's equations for determining electric current distributions inside submerged arc furnaces. A 3D finite volume model has been developed in ANSYS Fluent and implemented using User Define Scalar (UDS). We have considered a simplified furnace that consists of three electrodes and check the validity of the simulation results based on the skin-effect and the proximity effect. The results show that the proposed method can handle these effects. As a future work the proposed method will be applied to a real industrial submerged arc furnace that contains several components such as electrodes, arcs, crater and crater wall.

Acknowledgments. The Icelandic Technology development fund is greatly acknowledged for their funding of this work.

References

1. Krokstad, M.: Electrical resistivity of industrial SiC crusts. MSc-thesis, NTNU (2014)
2. Vangskåsen, J.: Metal-producing mechanisms in the carbothermic silicon process. MSc. thesis, NTNU (2012)
3. Mølnås, H.: Investigation of SiO condensate formation in the silicon process. Project report in TMT 4500. NTNU, Norway (2010)
4. Nell, J., Joubert, C.: Phase Chemistry of digout samples from a ferrosilicon furnace. In: The 13th International Ferroalloys Congress, pp. 265–271. Almaty, Kazakhstan (2013)
5. Palsson, H., Jonsson, M.: Finite element analysis of proximity effects in Soderberg electrodes. https://www.hi.is/~magnusj/ritverk/proximit.pdf. Accessed 07 Jan 2018
6. Toh, T., Yamasaki, N., Seki, T., Tanaka, J.: Magnetohydrodynamic simulation in steel making process by 3D finite element method. In: Proceedings of the 4th International Conference on CFD in the Minerals and Process Industries SINTEF/NTNU. Trondheim, Norway (2005)
7. Dhainaut, M.: Simulation of the electric field in a submerged arc furnace. In: Proceedings of the 10th International Ferroalloys Congress, pp. 605–613. Cape Town, South Africa (2004)
8. Bezuidenhout, J.J., Eksteen, J.J., Bardshaw, S.M.: Computational fluid dynamic modelling of an electric furnace used in the smelting of PGM containing concentrates. Miner. Eng. **22** (11), 995–1006 (2009)
9. Darmana, D., Olsen, J.E., Tang, K., Ringldalen, E.: Modelling concept for submerged arc furnaces. In: Proceedings of the 9th International Conference on CFD in the Minerals and Process Industries CSIRO. Melbourne, Australia (2012)
10. Wang, Z., Fu, Y., Wang, N., Feng, L.: 3D numerical simulation of electric arc furnaces for the MgO production. J. Mat. Pro. Tec. **214**(11), 2284–2291 (2014)
11. FLUENT, ver. 17.0, ANSYS Inc., Southpointe, 275 Technology Drive, Canonsburg, PA 15317 (2017)
12. Schei, A., Tuset, J.K., Tveit, H.: Production of high silicon alloys. Tapir Forlag, Trondheim (1998)
13. Sævarsdottir, G.A., Bakken, J.A., Sevastyanenko, V.G., Liping, G.: High power AC arcs in metallurgical furnaces. High Temp. Mater. Process. **5**(1) (2001)

14. Saevarsdottir, G.A., Bakken, J.A.: Current distribution in submerged arc furnaces for silicon metal/ferrosilicon production. In: Proceedings of the 12th International Ferroalloys Congress, pp. 717–728. Helsinki, Finland (2010)
15. Tranell, G., Andersson, M., Ringdalen, E., Ostrovski, O., Stenmo, J.J.: Reaction zones in a FeSi75 furnace – results from an industrial excavation. In: Proceedings of the 12th International Ferroalloys Congress, pp. 709–715. Helsinki, Finland (2010)
16. Myrhaug, E.H.: Non-fossil reduction materials in the silicon process -properties and behavior. Ph.D. thesis, NTNU (2003)
17. Tangstad, M., Ksiazek, M., Andersen, J.E.: Zones and materials in the Si furnace. In: Silicon for the Chemical and Solar Industry XII. Trondheim, Norway (2014)
18. Griffiths, D.J., College, R.: Introduction to Electrodynamics, 3rd edn. Prentice-Hall Inc., USA (1999)
19. ICEM-CFD, ver . 17.0, ANSYS Inc., Southpointe, 275 Technology Drive, Canonsburg, PA 15317 (2017)